International Journal of Humanoid Robotics
Vol. 15, No. 2 (2018) 1850010 (33 pages)

DOI: 10.1142/S021984361850010X

World Scientific
www.worldscientific.com

Modeling and Path-Following Control of a Wheelchair in Human-Shared Environments

Daniel Herrera*, Flavio Roberti† and Ricardo Carelli‡
Instituto de Automática, Universidad Nacional de San Juan — CONICET,
Av. Libertador Oeste 1109, San Juan, Argentina
*dherrera@inaut.unsj.edu.ar
†froberti@inaut.unsj.edu.ar
‡rcarelli@inaut.unsj.edu.ar

Victor Andaluz§, José Varela and Jessica Ortiz
Universidad de las Fuerzas Armadas, Ecuador
§vhandaluz1@espe.edu.ec

Paúl Canseco
Universidad Técnica de Ambato, Ecuador

Received 29 April 2017
Accepted 15 November 2017
Published 15 March 2018

This work presents the kinematic and dynamic modeling of a human–wheelchair system which considers that its center of mass is not located in the middle of the wheel's axle. Furthermore, a novel motion controller is presented for a human–wheelchair system, which is capable of performing positioning and path-following tasks in human-shared environments. This controller design is based on two cascaded subsystems: a kinematic controller, and a dynamic controller that compensates the dynamics of the human–wheelchair system. Additionally, an algorithm based on fuzzy-logic is proposed and incorporated in the aforementioned path-following control for pedestrian collision avoidance. This methodology considers to quantify heuristics social rules to make a balance between modulating velocity or direction during the avoidance. Three different interference cases, commonly found during walking events, are tested in a structured scenario. The experimental results demonstrate that the system is capable of overcoming many usual interference situations with human obstacles. A good performance of the path-following control is also verified.

Keywords: Wheelchair; dynamic modeling; cascade control; Lyapunov's method; fuzzy logic; social evasion; pedestrian collision avoidance; human–robot interaction.

1. Introduction

In recent years, robotics research has experienced a significant change. Research interests are now moving from the development of robots for structured industrial

† Corresponding author.

environments to the development of autonomous mobile robots operating in unstructured and natural environments.[1–6] The integration of robotic issues into the medical field has shown growing interest in recent years. Service, assistance, rehabilitation and surgery are some of the human health-care areas which have been benefited with the recent advances in robotics. Specifically, autonomous and safe navigation of wheelchairs in human-shared environments is a critical goal in assistance robotics.[1–4,7–10]

A robotic wheelchair assists people with both lower and upper limb impairments or severe motor dysfunctions to overcome the difficulties in self-driving a wheelchair. The robotic wheelchair system integrates a sensory subsystem, a navigation and control module and a user-machine interface to guide the wheelchair in autonomous or semi-autonomous mode.[7–9] In autonomous mode, the robotic wheelchair moves to the destination without user-control. This mode is intended for people who have great difficulties to drive the wheelchair. In semi-autonomous mode, the user shares the control with the robotic wheelchair. In this case, some motor skills of the user are needed.

Hence, a trajectory will be automatically generated and a trajectory tracking control will guide the wheelchair to the desired target. As indicated, the fundamental problems of motion control of a robotic wheelchair can be roughly classified into three groups: (1) point stabilization control: the objective is to stabilize the wheelchair at a target point with a desired heading; (2) trajectory tracking control: the wheelchair is required to track a time-parametrized reference; and (3) path-following control: the wheelchair is required to converge to a path and to follow it, without any time specifications. This work is focused on the path-following control problem.[11] The path-following control problem has been well studied in the literature, and many solutions have been proposed and applied in a wide range of applications.

Let $\mathcal{L}_d(s) \in \mathcal{R}^2$ be a desired geometric path parametrized by the curvilinear abscissa $s \in \mathcal{R}$. In the literature, different control algorithms for path-following control consider $s(t)$ as an additional control input.[12–15] Furthermore, it is important to consider the wheelchair's dynamics in addition to its kinematics because wheelchairs carry relatively heavy loads. As an example, the trajectory tracking task can be severely affected by the change imposed to the wheelchair dynamics when it is carrying a person, as shown in Martins *et al.*[16] Hence, some path-following control architectures already proposed in the literature have considered the inclusion of the dynamics of the wheelchair robots.[10,17] In such context, it is important to indicate that the mass center of the robotic wheelchair changes because of postural issues, limb amputations, or obesity.[18]

When a social robot (a human–wheelchair system) navigates in a human-shared environment, it is supposed that it must respect social zones of human obstacles to improve its social acceptance. As consequence of this hypothesis, in robotics, some conventions have been established. For example, Lam *et al.*[19] discuss different types of personal space for humans according to the situation, e.g., they assume an egg-shaped personal space for the human while walking, due to the fact that they should

have a long and clear space during the gait (so as to render the feeling of being safe). As a result, they consider that the length of the semi-major axis of the potential field is proportional to the human velocity. Scandolo and Fraichard use personal space in their social cost map model for path simulation.[20] Guzzi *et al.*[21] incorporate a potential field that dynamically modifies its dimensions according to the relative distance to the human to avoid an occlusion event or a "deadlock". In Ratsamee *et al.*[22] a human-friendly navigation approach is proposed, where the concept of personal space or "hidden space" is used to prevent uncomfortable feelings when humans try to avoid or interact with robots. This is based on the analysis of human motion and behavior (face orientation and overlapping of personal space).

In recent years, many works have focused in solving this kind of problem in human-shared environments. The social force model is probably the first model for pedestrians, which is capable of predicting the emergence of collective, self-organized crowd patterns from local interactions among individuals.[23] Since its first publication in 1995, there has been an important development of this model as well as new models based on similar concepts.[22] Consequently, in current times, the social force model is largely seen as a general framework commonly used in the community of crowd modelers.[24]

In addition, some specific scenarios have been studied during the locomotion in corridors and intersections between humans, commonly named as "passing" and "crossing" events, respectively. To represent these behaviors, both of them have been studied separately by considering modifications over the traditional functional cost for navigation based on global planification, where the functional cost is modified according to the *direction compatibility*. This approach allows to modulate speed instead of wheelchair heading when avoiding pedestrian collision. These algorithms are based on the projection of human motion. However, the global planification perspective requires, consequently, high computational costs.[25,26]

In contrast, other authors consider totally decentralized algorithms,[21,27] as an extension of bio-inspired cognitive simulation methods, e.g., the algorithm developed to simulate crowd of humans.[28] These algorithms consider the projection of the robot and all the individuals in the scenario by considering a uniform linear motion, which allows to generate a collision curve for each participant, whereon the distances of collision in each direction of motion are represented. In this way, each individual moves in a direction without colliding and where the objective point is the nearest one. This bio-inspired algorithm has proven useful for many crowd simulations, even though the high computational costs are also a hindrance to a practical implementation. Although many approaches have presented alternatives to avoid humans in different scenarios, they are focused in crowd simulation, and its extension to the mobile robot field has resulted quite limited. Besides, no methodology has been presented that allows for incorporating this locomotion behavior in a physical platform as a reactive and decentralized algorithm. The decentralized approach based on bio-inspired and heuristic algorithms seems the most likely reliable method to apply in this kind of social navigation tasks.

Therefore, this work presents a control algorithm for autonomous navigation of a human–wheelchair system to assist persons with severe motor disabilities, which is able to follow a path in human-shared environments. In this way, the assistive device does not only increase the autonomy of people with motor disabilities but also contributes to their social inclusion. The proposal consists of a control algorithm to follow the path, and a heuristic algorithm to modify the path references according to an inferred collision avoidance strategy. For this, a dynamic model of the human–wheelchair system which considers lateral deviations of the mass center sourced to user's movement, limb amputations, or obesity, is considered. The obtained dynamic model has an adequate structure and properties for designing a control law, and the control input can be given in terms of linear and angular reference velocities, as usually found in commercial mobile robots.[10] This latter characteristic is an advantage when evaluating the control experimentally. In this manner, the path following control consists of a cascade control scheme, where: (i) the outer-loop consists of a kinematic controller with saturation of velocity commands, which is based on wheelchair robot's kinematic; and (ii) the inner-loop consists of a dynamic compensation controller that considers the aforementioned dynamic model, which is directly related to physical parameters of the system. The stability of the proposed control system is proven through Lyapunov's method.

Once that the path-following control is guaranteed, a novel heuristic human-evasion avoidance algorithm is included to modify the desired path reference, where the concept of social navigation is mainly analyzed as an alternative to improve the acceptance, performance and autonomy of robotic wheelchair systems. The legibility of the robot motions is a key point to be improved, i.e., improve the means to make a person intuitively understands the intentions of a robot.[25,29] Particularly, this novel heuristic approach quantifies social rules that are commonly used by pedestrians in locomotion situations, i.e., passing in corridors or crossing in intersections, where a nonverbal negotiation is required. The main objective is to define an algorithm based on fuzzy-logic to make a balance between speed variation and wheelchair heading changes to avoid pedestrian collision. In this way, the methodology consists in analyzing the movement characteristics, such as the relative location, orientation and distance between the human obstacle and the human–wheelchair system, and generating rules that define legible and natural movements, easily predictable by humans. In consequence, a methodology to incorporate this effect in the path-following control based on a social force composition is proposed. Finally, to validate the proposed control algorithm, experimental results are included and discussed.

The paper is organized as follows: Section 2 shows the modeling of the human–wheelchair system. Section 3 describes the path following's formulation problem and the control scheme. System stability is also analyzed in this section. Later, Sec. 4 gives a detailed description of the fuzzy-based algorithm for pedestrian collision avoidance by considering its incorporation in the path-following control. In Sec. 5, three different interference scenarios are tested to verify the performance of this

method. As a result, a brief discussion about the experimental results is presented in Sec. 6. Finally, conclusions are given in Sec. 7.

2. Modeling of a Human–Wheelchair System

As aforementioned, this work is based on a human–wheelchair system. A robotic wheelchair is a differential drive mobile robot (DDMR) that can rotate freely around its vertical axis. It is assumed that the human–wheelchair system moves on a planar horizontal surface, where the vertical disturbances have been neglected (see Fig. 1 and its nomenclature in Table 1).

Let $\mathcal{R}(\mathcal{X}, \mathcal{Y}, \mathcal{Z})$ be any fixed frame with $\mathcal{Z}$ vertical axis. Traditionally, the motion control design for DDMR has considered that the point of interest, which should follow a desired trajectory, is located at the middle of a virtual axle between the wheels. However, in this work, this point is located in front of the virtual axle (point $h(x, y)$ of Fig. 1). Such point is herein after named as the point of interest. Figure 1 illustrates the wheelchair considered in this work.

The force and moment equations for the human–wheelchair system are:

$$\sum F_{x'} = m(\dot{u}' - \bar{u}\omega) = F_{rlx'} + F_{rrx'} + F_{cx'} + F_{dx'} + F_{ex'} + F_{fx'}, \tag{1}$$

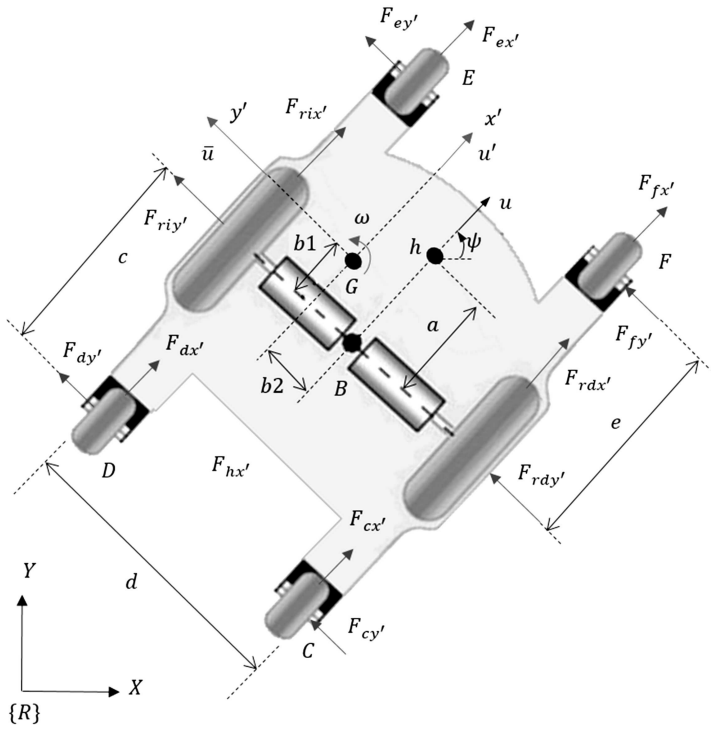

Fig. 1. Schematic of the robotic wheelchair.

Table 1. Nomenclature of the schematic of the wheelchair.

G	Center of mass
B	The center axis of the two wheels
$h(x, y)$	Point that is required to track a path in $\mathcal{R}$
x, y	Position in the axes of the wheelchair
ψ	Robotic wheelchair heading
ω	Angular velocity
$u', \bar{u}$	Longitudinal and lateral velocities of the center of mass
$F_{rrx'}, F_{rry'}$	Longitudinal and lateral tire forces of the right wheel
$F_{rlx'}, F_{rly'}$	Longitudinal and lateral tire forces of the left wheel
$F_{hx'}, F_{hy'}$	Longitudinal and lateral force exerted on, by the human
τ_h	Moment exerted by the human
$F_{cx'}, F_{cy'}, F_{dx'}, F_{dy'}$	Longitudinal and lateral tire forces exerted on C and D by the rear castor wheels
$F_{ex'}, F_{ey'}, F_{fx'}, F_{fy'}$	Longitudinal and lateral tire forces exerted on E and F by the front castor wheels
d, b_1, b_2, a, c	Distances

$$\sum F_{y'} = m(\dot{\bar{u}} - u'\omega) = F_{rly'} + F_{rry'} + F_{cy'} + F_{dy'} + F_{ey'} + F_{fy'}, \tag{2}$$

$$\begin{aligned}\sum M_z = I_z\dot{\omega} = \frac{d}{2}(F_{rrx'} - F_{rlx'}) + b_2(F_{rrx'} + F_{rlx'}) - b_1(F_{rly'} + F_{rry'}) \\ - (c - b_1)(F_{dy'} + F_{cy'}) + (e - b_1)(F_{fy'} + F_{ey'}) + \left(\frac{d}{2} + b_2\right)(F_{cx'} \\ + F_{fx'}) - \left(\frac{d}{2} - b_2\right)(F_{dx'} + F_{ex'}),\end{aligned} \tag{3}$$

where $m = m_h + m_w$ is the human–wheelchair system mass in which m_h is the human mass and m_w is the wheelchair mass; and I_z is the human–wheelchair system moment of inertia about the vertical axis located in G. According to Zhang *et al.*[30] velocities u, ω and $\bar{u}$, including the slip speeds, are given by

$$u = \frac{r}{2}(\omega_r + \omega_l); \quad \omega = \frac{r}{d}(\omega_r - \omega_l), \tag{4}$$

$$\bar{u} = b_1\omega, \tag{5}$$

where r is the right and left wheel radii; d is the distance between wheels; ω_r and ω_l are the angular velocities of the right and left wheels, respectively.

It is considered that motors of the wheelchair are identical, thus, the motor models attained by neglecting the voltage on the inductances are:

$$\tau_r = \frac{k_a(v_r - k_b\omega_r)}{R_a}; \quad \tau_l = \frac{k_a(v_l - k_b\omega_l)}{R_a}, \tag{6}$$

where v_r and v_l are the input voltages applied to the right and left motors; k_b is equal to the voltage constant multiplied by the gear ratio; R_a is the electric resistance constant; τ_r and τ_l are the right and left motor torques multiplied by the gear ratio; and k_a is the torque constant multiplied by the gear ratio. The dynamic equations of the motor-wheels are:

$$I_e\dot{\omega}_r + B_e\omega_r = \tau_r - F_{rrx'}r, \tag{7}$$

$$I_e\dot{\omega}_l + B_e\omega_l = \tau_l - F_{rlx'}r, \tag{8}$$

where I_e and B_e are the moment of inertia and the viscous friction coefficient of the combined motor rotor, gearbox, and wheel. In general, commercial robots have low-level controllers based on PID controllers to track commands of angular and linear velocity. Therefore, it is useful to express the human–wheelchair system model in a suitable way by considering rotational and translation velocity references as input signals. For this purpose, the velocity controllers are included into the model. To simplify the model, a PD velocity controller has been considered, which is described by the following equations:

$$v_u = k_{\mathrm{PT}}(u_{\mathrm{ref}} - u_{\mathrm{me}}) + k_{\mathrm{DT}}(\dot{u}_{\mathrm{ref}} - \dot{u}_{\mathrm{me}}), \tag{9}$$

$$v_\omega = k_{\mathrm{PR}}(\omega_{\mathrm{ref}} - \omega_{\mathrm{me}}) + k_{\mathrm{DR}}(\dot{\omega}_{\mathrm{ref}} - \dot{\omega}_{\mathrm{me}}), \tag{10}$$

where k_{PT}, k_{DT}, k_{PR} and k_{DR} are gain positive constants of the PD controllers.

Later, from (1)–(10) and neglecting perturbations and uncertainties, the dynamic model of the human–wheelchair system is obtained and compactly expressed as:

$$\mathbf{M}(\varsigma)\dot{\mathbf{v}} + \mathbf{C}(\varsigma, \mathbf{v})\mathbf{v} = \mathbf{v_{ref}}, \tag{11}$$

where $\mathbf{M}(\varsigma) \in \Re^{nxn}$ with $n = 2$ and $\mathbf{M}(\varsigma) = \begin{bmatrix} \varsigma_1 & -\varsigma_7 \\ -\varsigma_8 & \varsigma_2 \end{bmatrix}$ represents the human–wheelchair system's inertia; $\mathbf{C}(\varsigma, \mathbf{v}) \in \Re^{nxn}$ and $\mathbf{C}(\varsigma, \mathbf{v}) = \begin{bmatrix} \varsigma_4 & -\varsigma_3\omega \\ \varsigma_5\omega & \varsigma_6 \end{bmatrix}$ represents the components of the centripetal forces; $\mathbf{v} \in \Re^n$ and $\mathbf{v} = [u\ \omega]^T$ is the vector of system's velocity; $\mathbf{v}_{\mathrm{ref}} \in \Re^n$ and $\mathbf{v_{ref}} = [u_{\mathrm{ref}}\ \omega_{\mathrm{ref}}]^T$ is the vector of velocity control signals for the wheelchair; and $\varsigma \in \Re^l$ with $l = 8$ and $\varsigma = [\varsigma_1\ \varsigma_2\ \ldots\ \varsigma_l]^T$ is the vector of dynamic parameters, which contain the physical, mechanical and electrical parameters of the human–wheelchair dynamics. More details about these parameters and properties of this dynamic model with velocity references as control inputs can be found in Andaluz *et al.*[31]

2.1. *Kinematic expressions*

The kinematic expressions of the nonholonomic human–wheelchair system are defined as

$$\begin{cases} \dot{x} = u\cos\psi - a\omega\sin\psi \\ \dot{y} = u\sin\psi + a\omega\cos\psi \\ \dot{\psi} = \omega \end{cases}. \tag{12}$$

Also, the equation system (12) can be written compactly as

$$\begin{aligned} \dot{\mathbf{h}} &= \mathbf{J}(\psi)\mathbf{v}, \\ \dot{\psi} &= \omega, \end{aligned} \tag{13}$$

where $\dot{\mathbf{h}} = [\dot{x}\ \dot{y}]^{\mathrm{T}} \in \Re^2$ represents the vector of axis velocity of the $\mathcal{R}(\mathcal{X}, \mathcal{Y}, \mathcal{Z})$ system; $\mathbf{J}(\psi) = \begin{bmatrix} \cos\psi & a\sin\psi \\ \sin\psi & a\cos\psi \end{bmatrix} \in \Re^{2x2}$ is a singular matrix; and the control of maneuverability of the wheelchair is defined $\mathbf{v} \in \Re^n$ and $\mathbf{v} = [u\ \omega]^T \in \Re^2$ in which u and ω represent the linear and angular velocities of the wheelchair, respectively. Additionally, Eq. (12) includes the nonholonomic velocity constraint of the robotic wheelchair which determines that it can only move perpendicular to the wheels axle,

$$\dot{x}\sin\psi - \dot{y}\cos\psi + a\omega = 0. \tag{14}$$

Hence, the mathematical model of the human–wheelchair system is represented by (11) and (13), which represent the dynamic and kinematic model respectively, where the velocity references of the robotic wheelchair are the input signals.

3. Path Following and Positioning Controller

As represented in Fig. 2, the path to be followed is denoted as $\mathcal{P}(s)$, where $\mathcal{P}(s) = (x_P(s), y_P(s))$; the actual desired location $\mathcal{P}_d = (x_P(s_D), y_P(s_D))$ is defined as the closest point on $\mathcal{P}(s)$ to the human–wheelchair system, with s_D being the curvilinear abscissa defining the point $\mathcal{P}_d$; the unit vector tangent to the path in the point $\mathcal{P}_d$ is denoted by $\mathbf{T}$; θ_T is the orientation of $\mathbf{T}$ with respect to the inertial frame $\mathcal{R}(\mathcal{X}, \mathcal{Y}, \mathcal{Z})$;$\tilde{x} = x_P(s_D) - x$ is the position error in the $\mathcal{X}$ direction; $\tilde{y} = y_P(s_D) - y$ is the position error in the $\mathcal{Y}$ direction; $\boldsymbol{\rho}$ represents the distance between the wheelchair position $h(x, y)$ and the desired point $\mathcal{P}_d$, where the position error in the $\boldsymbol{\rho}$ direction is $\tilde{\rho} = 0 - \rho = -\rho$, i.e., the desired distance between the wheelchair position $h(x, y)$ and the desired point $\mathcal{P}_d$ must be zero; and θ_ρ is the orientation of the error vector $\tilde{\rho}$ with respect to the inertial frame $\mathcal{R}(\mathcal{X}, \mathcal{Y}, \mathcal{Z})$.

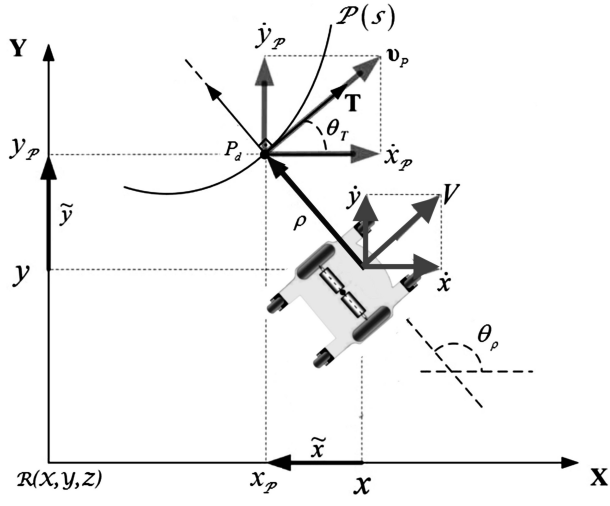

Fig. 2. The orthogonal projection of the point of interest over the path.

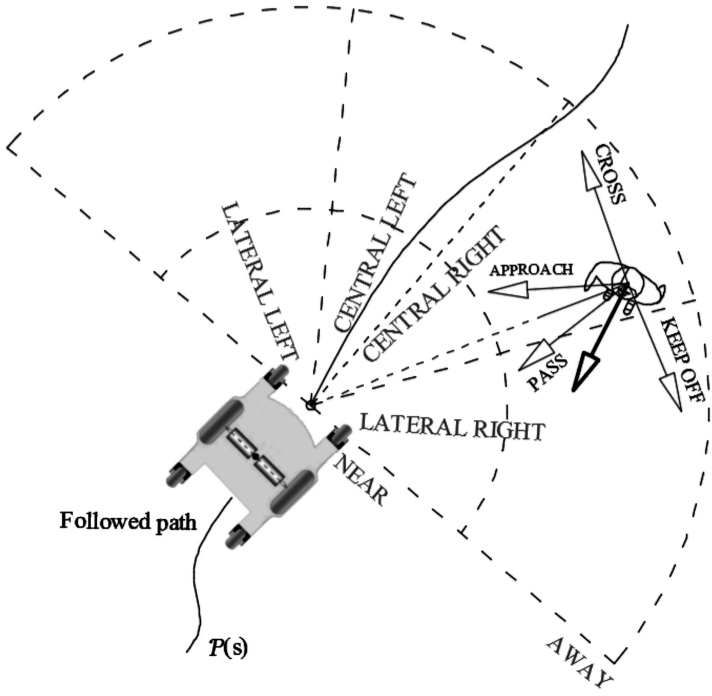

Fig. 3. Fuzzy inputs used to define social rules.

According to Fig. 8, the path-following problem is solved by a control law capable of making the point of interest to assume a desired velocity equal to

$$V = \upsilon_P(s_D, h) = |\upsilon_P(s_D, h)| \measuredangle \theta_T, \tag{15}$$

besides making the human–wheelchair system stays on the path, i.e., $\tilde{x} = 0$ and $\tilde{y} = 0$. Therefore, if $\lim_{t\to\infty} \tilde{x}(t) = \mathbf{0}$ and $\lim_{t\to\infty} \tilde{y}(t) = \mathbf{0}$, then $\lim_{t\to\infty} \rho(t) = 0$ and $\lim_{t\to\infty} \tilde{\psi}(t) = 0$, being $\tilde{\psi}$ the orientation error of the wheelchair, defined as $\tilde{\psi} = \theta_T - \psi$.

It is worth noting that the desired velocity reference $\upsilon_P(s_D, h)$ of the wheelchair during the tracking path could not be constant, as it is common in the literature,[1,3,10,14–16]

$$\upsilon_P(s_D, h) = f(k, s_D, \rho(t), \omega(t), \ldots), \tag{16}$$

the wheelchair's desired velocity can be expressed as: constant function, curvilinear abscissa function of the path, position error function, angular velocities function of the wheelchair; and many others.

Remark 1. Notice that the positioning problem is a particular case of path-following, for which $\upsilon_P(s_D, h) = 0$.

3.1. *Structure of the controller*

The structure of the controller here proposed for the path following and positioning problems, shown in Fig. 5, the design of the controller is based mainly on two cascaded subsystems: (1) Kinematic controller where the control errors $\rho(t)$ and $\tilde{\psi}(t)$ may be calculated at every measurement time and used to drive the mobile robot in a direction which decreases the errors; and (2) Dynamic compensation controller, whose main objective is to compensate the dynamics of the human–wheelchair system, thus reducing the velocity tracking error.

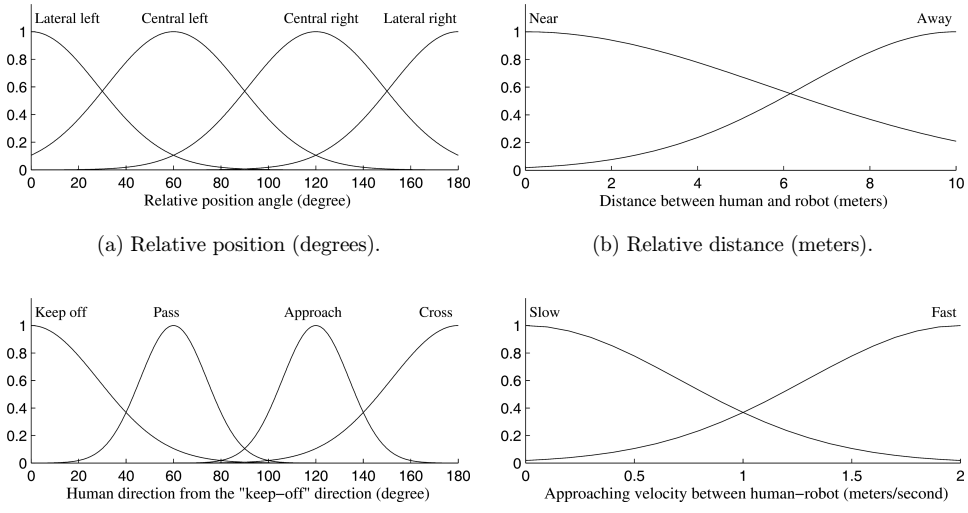

(a) Relative position (degrees).

(b) Relative distance (meters).

(c) Relative Orientation (degrees).

(d) Relative velocity (m/s).

Fig. 4. Membership functions of the fuzzy inputs.

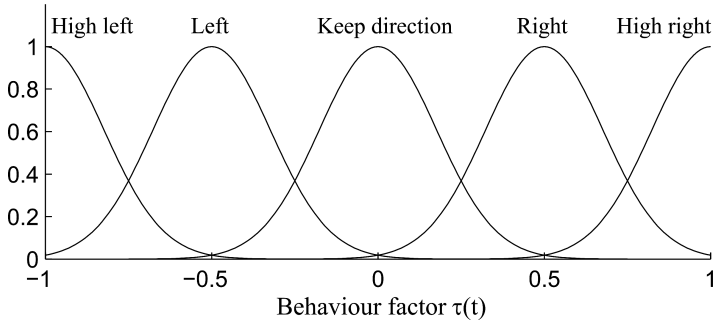

Fig. 5. Membership functions of the fuzzy output.

3.1.1. *Kinematic controller*

The proposed kinematic controller is based on the kinematic model of the wheelchair (12), i.e., $\dot{\mathbf{h}} = \mathbf{J}(\psi)\mathbf{v}$. Hence, following control law is proposed,

$$\begin{bmatrix} u_c \\ \omega_c \end{bmatrix} = \mathbf{J^{-1}}\left(\begin{bmatrix} \dot{x}_P \\ \dot{y}_P \end{bmatrix} + \begin{bmatrix} \rho_x \\ \rho_y \end{bmatrix} \right), \tag{17}$$

with,

$$\dot{x}_P = |\upsilon_P| \cos(\theta_T), \quad \text{and} \quad \dot{y}_P = |\upsilon_P| \sin(\theta_T), \tag{18}$$

where u_c and ω_c are the velocities outputs of the kinematic controller, υ_P is the reference velocity input of the wheelchair for the controller, $\dot{x}_P$ is the projection of υ_P in the $\mathcal{X}$ direction, $\dot{y}_P$ is the projection of υ_P in the $\mathcal{Y}$ direction, $\mathbf{J^{-1}}$ is the matrix of inverse kinematics for the wheelchair, and ρ_x and ρ_y are the position error in the $\mathcal{X}$ and $\mathcal{Y}$ direction, respectively, respect to the inertial frame $\mathcal{R}(\mathcal{X}, \mathcal{Y}, \mathcal{Z})$. In order to include an analytic saturation of velocities in the wheelchair, the $\tanh(.)$ function is included, which limits the errors ρ_x and ρ_y. Hence, it is defined as,

$$\rho_x = l_x \tanh\left(\frac{k_x}{l_x}\tilde{x}\right), \quad \text{and} \quad \rho_y = l_y \tanh\left(\frac{k_y}{l_y}\tilde{y}\right). \tag{19}$$

where k_x, k_y, l_x and l_y are positive design constants that weigh the control error and avoid actuators saturation. Now, the behavior of the control position error of the wheelchair is analyzed by assuming -by now- perfect velocity tracking, i.e., $u(t) \equiv u_c(t)$ and $\omega(t) \equiv \omega_c(t)$. In this manner, by substituting Eqs. (13) in (17), the closed-loop response of the external loop is expressed by

$$\begin{bmatrix} \dot{x} \\ \dot{y} \end{bmatrix} = \begin{bmatrix} \dot{x}_P \\ \dot{y}_P \end{bmatrix} + \begin{bmatrix} l_x \tanh\left(\frac{k_x}{l_x}\tilde{x}\right) \\ l_y \tanh\left(\frac{k_y}{l_y}\tilde{y}\right) \end{bmatrix}, \tag{20}$$

The analysis of the stability of the closed-loop system considers the following relations from Fig. 2,

$$\tilde{x} = -\tilde{\rho}\sin(\theta_T), \quad \text{and} \quad \tilde{y} = \tilde{\rho}\cos(\theta_T). \tag{21}$$

Furthermore,

$$\dot{\rho} = -\dot{x}\sin(\theta_T) + \dot{y}\cos(\theta_T). \tag{22}$$

If $\tilde{\rho} = -\rho$, then its time derivative is,

$$\dot{\tilde{\rho}} = -\dot{\rho}, \tag{23}$$

and substituting Eq. (22) in Eq. (23), it results,

$$\dot{\tilde{\rho}} = \dot{x}\sin(\theta_T) - \dot{y}\cos(\theta_T), \tag{24}$$

On the other hand, introducing Eqs. (18) and (20) in Eq. (24), one gets

$$\dot{\tilde{\rho}} = l_x \tanh\left(\frac{k_x}{l_x}\tilde{x}\right)\sin(\theta_T) - l_y \tanh\left(\frac{k_y}{l_y}\tilde{y}\right)\cos(\theta_T), \tag{25}$$

Finally, the behavior of $\tilde{\rho}$ for the closed-loop system is obtained by substituting Eq. (21) into Eq. (25), which is written as,

$$\dot{\tilde{\rho}} = l_x \tanh\left(-\tilde{\rho}\frac{k_x}{l_x}\sin(\theta_T)\right)\sin(\theta_T) - l_y \tanh\left(\tilde{\rho}\frac{k_y}{l_y}\cos(\theta_T)\right)\cos(\theta_T). \tag{26}$$

Remark 2. From Eq. (26), it can be concluded that such a system has only one equilibrium point, which is $\tilde{\rho} = 0$.

For the stability analysis, the following Lyapunov candidate function is considered $V(\tilde{\rho}) = \frac{1}{2}\tilde{\rho}^2 > 0$. Its time derivative on the trajectories of the system is $\dot{V}(\tilde{\rho}) = \tilde{\rho}\dot{\tilde{\rho}}$, a sufficient condition for the stability of the equilibrium of the close-loop system is that $\dot{V}(\tilde{\rho})$ is a negative-definite function. Then, introducing the closed-loop system of the Eq. (26) in $\dot{V}(\tilde{\rho})$, results

$$\dot{V}(\tilde{\rho}) = \tilde{\rho} l_x \tanh\left(-\tilde{\rho}\frac{k_x}{l_x}\sin(\theta_T)\right)\sin(\theta_T) - \tilde{\rho} l_y \tanh\left(\tilde{\rho}\frac{k_y}{l_y}\cos(\theta_T)\right)\cos(\theta_T), \tag{27}$$

where $\dot{V}(\tilde{\rho}) < 0$, and in consequence, the stability of the closed-loop system is guaranteed if the gain constants of the controller that weigh the control error are also positive, i.e., $l_x > 0$, $k_x > 0$, $l_y > 0$ and $k_y > 0$. Hence, from Eq. (27), it is concluded that $\lim_{t\to\infty}\tilde{\rho}(t) \to 0$, i.e., $\tilde{x}(t) \to 0$ and $\tilde{y}(t) \to 0$ with $t \to \infty$ asymptotically. Therefore, from Eq. (20), it can be concluded that the final velocity of the point of interest will be $V = |\upsilon_P(s_D, h)|\measuredangle\theta_T$. Hence, $\tilde{\psi}(t) \to 0$ for $t \to \infty$ asymptotically.

Remark 3. Notice that for positioning tasks, i.e., $\upsilon_P(s_D, h) = 0$, when the human–wheelchair system reaches the target point it stays in that position (but, without the control of its final orientation).

3.1.2. *Dynamic compensation controller*

If the condition of perfect velocity tracking in the kinematic controller design is not considered, then $u(t) \neq u_c(t)$ and $\omega(t) \neq \omega_c(t)$. This velocity tracking error motivates the design of a dynamic compensation controller. The objective of this controller is to compensate the dynamic of the human and of the wheelchair, thus reducing the velocity tracking error. In this manner, a control law based on the dynamic model of Eq. (11) is proposed,

$$\begin{bmatrix} u_{\text{ref}} \\ \omega_{\text{ref}} \end{bmatrix} = \mathbf{M}\left(\begin{bmatrix} \dot{u}_c \\ \dot{\omega}_c \end{bmatrix} + \begin{bmatrix} \sigma_u \\ \sigma_\omega \end{bmatrix}\right) + \mathbf{C}\begin{bmatrix} u \\ \omega \end{bmatrix}, \tag{28}$$

with,

$$\sigma_u = l_u \tanh\left(\frac{k_u}{l_u}\tilde{u}\right), \quad \text{and} \quad \sigma_\omega = l_\omega \tanh\left(\frac{k_\omega}{l_\omega}\tilde{\omega}\right),$$

where $\tilde{u}(t) = u_c(t) - u(t)$, and $\tilde{\omega}(t) = \omega_c(t) - \omega(t)$ are the linear and angular velocity errors, respectively; $l_u > 0$, $k_u > 0$, $l_\omega > 0$ and $k_\omega > 0$ are positive gain constants that weigh the control error. By substituting Eq. (28) in Eq. (11), the closed-loop response of the system is expressed as,

$$\begin{bmatrix} \dot{u} \\ \dot{\omega} \end{bmatrix} = \begin{bmatrix} \dot{u}_c \\ \dot{\omega}_c \end{bmatrix} + \begin{bmatrix} l_u \tanh\left(\frac{k_u}{l_u}\tilde{u}\right) \\ l_\omega \tanh\left(\frac{k_\omega}{l_\omega}\tilde{\omega}\right) \end{bmatrix}. \tag{29}$$

Following with this, a Lyapunov candidate function and its time derivative on the system trajectories are introduced in order to consider the corresponding stability analysis $V(\tilde{u}, \tilde{\omega}) = \frac{1}{2}(\tilde{u}^2 + \tilde{\omega}^2) > 0$; the time derivative of the Lyapunov candidate function is,

$$\dot{V}(\tilde{u}, \tilde{\omega}) = \tilde{u}\dot{\tilde{u}} + \tilde{\omega}\dot{\tilde{\omega}}, \tag{30}$$

After introducing the derivative of Eq. (29) in Eq. (30), the time derivative $\dot{V}(\tilde{u}, \tilde{\omega})$ is now

$$\dot{V}(\tilde{u}, \tilde{\omega}) = -\tilde{u} l_u \tanh\left(\frac{k_u}{l_u}\tilde{u}\right) - \tilde{\omega} l_\omega \tanh\left(\frac{k_\omega}{l_\omega}\tilde{\omega}\right) < 0, \tag{31}$$

In this way, from Eq. (31), it is concluded that $\tilde{u}(t) \to 0$ and $\tilde{\omega}(t) \to 0$ with $t \to \infty$ asymptotically.

4. Pedestrian Collision Avoidance Based on Fuzzy Logic

Human locomotion in public spaces requires strategies to avoid collision with other pedestrians. In the bibliography, crowd modelers refer to these pedestrians as *interferers*. To avoid these individuals, humans modulate their direction, velocity or both of them. Currently, the literature is not conclusive of how humans adjust these two parameters in the presence of an interferer. This fact impedes the development of mathematical models which describe the human locomotion behavior during the interferers avoidance. Consequently, it results in difficulty to make a mobile robot able to emulate this human locomotion behavior.[32]

Our approach take advantage of the close relationship between the shape of the human gait paths in goal-directed movements and the simplified kinematic model of a wheeled mobile robot.[33] Under this assumption, the problem is only focused in the social rules to define a human locomotion behavior, that allows to make a balance between modulating velocity or/and direction. This locomotion behavior is only related to the decision during the locomotion, not to the motion dynamics itself.

In the following sections, a fuzzy logic approach is used to incorporate social rules for pedestrian collision avoidance in a suitable and adjustable way. To show its performance, the context of a path following control problem is considered.

4.1. *Quantification of human locomotion behavior during evasion*

4.1.1. *Fuzzy behavior rules*

This section describes the quantification of social rules through fuzzy rules, obtained in a heuristic way, to determine a human locomotion behavior. The output of these behaviors are fused to determine the tendency to two opposite behaviors, passing (prioritizing change of direction) and crossing (prioritizing change of velocity), which is later defuzzified to weigh the path adaptation in terms of velocity, direction, or both of them, thus guaranteeing a *human–friendly* evasion.

A first step consists in defining the inputs. For this, four variables have been considered (see Figs. 3 and 4):

- ***Relative position*:** consists of four frontal and lateral zones from the human–wheelchair system point of view. These zones were inspired on the peripheral vision of the human eye, which is a part of vision that occurs outside the very center of gaze.
- ***Relative orientation*:** consists of four different expected behaviors of the human obstacle relative to the human–wheelchair system, which are related with his predisposition to pass, keep off or cross the human–wheelchair system path, and even when the human wants to approach himself to the human–wheelchair system and generate direct interaction. Even though the estimation of human intention to interact is an interesting issue, it has not been considered in the present work.
- ***Relative distance*:** related with the relative distance between the human and the human–wheelchair system.
- ***Relative velocity*:** the approaching velocity between a human and the human–wheelchair system.

As unique output, a *behavior factor* with five possible states is considered: *high left*, *left*, *right* and *high right* deviation, which will guarantee a soft or strong direction change, and one more named *keep direction*, which usually prioritizes a velocity modulation to guarantee the evasion (see used membership functions in Fig. 5).

Passing Behavior Rules

A *passing behavior* can be usually found in corridor scenarios, where a frontal encounter is expected and it must be guaranteed the free walking space of each individual. In this manner, it is expected that the human–wheelchair system tends to adapt his path in terms of a direction change, moving away of the human gait. For this purpose, the first four fuzzy rules were designed (see Table 2).

Table 2. Fuzzy rules to define a sociable acceptable behavior.

	Relative position				Relative distance		Relative orientation				Relative velocity		Deviation (output)				
Rules	L.L.	C.L.	C.R.	L.R.	Near	Away	K.O.	Pass	Appr.	Cross	Slow	Fast	H.L.	L.	K.D.	R.	H.R.
1			√		√			√					√				
2			√			√		√						√			
3		√			√			√									√
4		√				√		√								√	
5				√		√				√		√					√
6				√	√					√		√				√	
7				√		√				√	√					√	
8				√	√					√	√				√		
9	√					√				√		√	√				
10	√				√					√		√		√			
11	√					√				√	√			√			
12	√				√					√	√				√		
13									√						√		
14							√								√		

Notes: L.L=Lateral left, C.L.=Central Left, C.R.=Central Right, L.R.=Lateral Right, K.O.=Keep off, Appr.=Aproach, H.L.=High Left, L.=Left, K.D.=Keep direction, R.=Right, H.R.=High right.

Crossing Behavior Rules

The *crossing behavior* is usually found in the intersection of paths or corridors, where a nonverbal negotiation is developed to define: who waits and who passes through. In this case, the human–wheelchair system is always playing a passive role (by security reasons). As a result, the next eight fuzzy rules (5–12) have been designed to weigh the adaptation of the path as a combination of direction and velocity change. For this, the relative velocity and distance are also taken into account to generate a motion of *passing behind* the human.

The last two rules are defined considering another two human behaviors: human moving away and approaching him\herself to the human–wheelchair system. In these cases, a *keep direction* effect is expected. In the first one, the social force is possibly near or equal to zero, but in the second one, a velocity adaptation is generated to guarantee a passive interaction mode.

4.1.2. *Social zone for human obstacle*

If the pose of the human is $(\mathbf{x}_h, \theta_h)$, then the social zone of the human is defined as

$$\mathbf{x}_e(\theta_e) = \begin{bmatrix} x_e(\theta_e) \\ y_e(\theta_e) \end{bmatrix} = \mathbf{x}_h + \mathbf{R} \begin{bmatrix} m_a \cos(\theta_e) \\ m_i \sin(\theta_e) \end{bmatrix}$$

$$\text{being } \mathbf{R} = \begin{bmatrix} \cos\theta_h & -\sin\theta_h \\ \sin\theta_h & \cos\theta_h \end{bmatrix},$$

that represents the positions of the points on the personal space of the human (an ellipse rotated by $\mathbf{R}$ and with center in $\mathbf{x}_h$), distributed by angle, θ_e (varying from 0–2π). m_i and m_a are the minor and major axes, respectively. This shape of the human social zone is commonly found in the bibliography.

4.1.3. *Social force model*

In a shared environment, social forces of objects or the other humans are present. In this way, a human tends to adapt his/her direction or velocity according to these disturbances, which have been traditionally modeled as repulsive forces. A novel composition of this force to react in a social fashion is proposed, where the predisposition between the aforementioned two opposite behaviors, i.e., passing or crossing, is given by a defuzzified fuzzy logic output that allows to weigh two forces, which characterize a compound behavior. These force components act over the human–wheelchair system velocity and over the shape of the path, allowing to avoid in a social and reliable fashion the individual. Therefore, the resulting social forces are modeled as follows:

The magnitude of the repulsive social force is defined as[23]:

$$f_{\text{social}}(t) = \begin{cases} -ae^{\frac{d(t)}{b}}, & d(t) \geq 0 \\ 0, & d(t) < 0 \end{cases},$$

where a and b are positive constants representing the magnitude and the range of the social force, and,

$$\begin{aligned} d(t) &= r_{\text{robot}} + r_{\text{human}}(t) - d_{h/r}(t), \\ r_{\text{robot}} &= \text{Radius of the circular social zone of the robot}, \\ d_{h/r}(t) &= \|\mathbf{x}_r - \mathbf{x}_h\|_2, \quad r_{\text{human}}(t) = \|\mathbf{x}_e(\theta_e) - \mathbf{x}_h\|_2, \end{aligned}$$

where $(\mathbf{x}_h, \theta_h)$ and $(\mathbf{x}_r, \theta_r)$ are the pose of the human and the wheelchair respectively, and, $\mathbf{x}_e(\theta_e)$ is a point on the elliptical social zone of the human in the direction θ_e of the human–wheelchair system.

Then, the social forces are defined as:

$$\mathbf{f}_v(t) = (1 - |\tau(t)|) f_{\text{social}}(t) \mathbf{v}_{v(t)}, \tag{32}$$

$$\mathbf{f}_N(t) = \tau(t) f_{\text{social}}(t) \mathbf{v}_N, \tag{33}$$

where $\mathbf{v}_N$ and $\mathbf{v}_{v(t)}$ are the normal direction to the path (see Fig. 6) and the human–wheelchair system velocity direction, respectively. Additionally, $\tau(t)$ is the defuzzified output variable (normalized between $[-1, 1]$), which determines the dominant *behavior factor* according to the social fuzzy rules (see Fig. 5). The defuzzification process is based on a Mamdani-type fuzzy inference system given by the Fuzzy Logic Toolbox$^{\text{TM}}$ of Matlab®, which calculates $\tau(t)$ in each sample time.

Hereby, the system robot/path is modified according to its predominant behavior. Therefore, if the desired location $\mathcal{P}_d = (x_P(s_D), y_P(s_D))$ is defined as the closest point on $\mathcal{P}(s)$, then $\mathcal{P}_d$ is modified by the social force during evasion as follows:

$$\mathcal{P}_d^* = \mathcal{P}_d + \Delta\mathcal{P}_d = \begin{pmatrix} x_P^* \\ y_P^* \end{pmatrix}, \quad \text{with, } \Delta\mathcal{P}_d = k_N \mathbf{f}_N,$$

where $k_N(t)$ in $[m/N]$ is a physical constant that weighs the relation between social force and path adaptation. Additionally, a simple filtering process is used to guarantee the smoothness of the path change. It consists in averaging the neighbor points

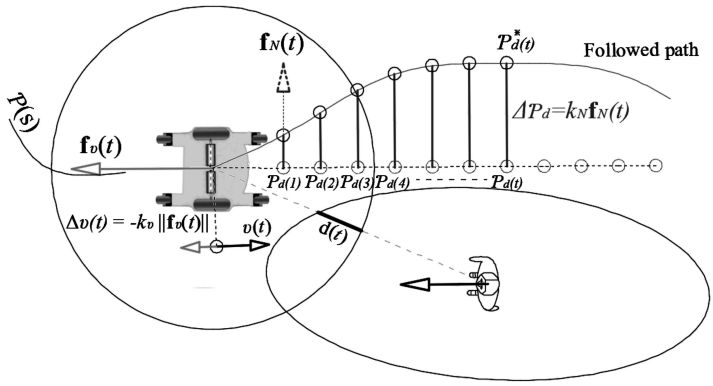

Fig. 6. Social force effect.

of $\mathcal{P}_d$ on the path with the resulting $\mathcal{P}_d^*$ and using this value to define the new path and calculate the control errors with (19).

In this way, the kinematic controller proposed in Eq. (17) results to be modified as follows:

$$\begin{bmatrix} u_c{}^* \\ \omega_c^* \end{bmatrix} = \mathbf{J}^{-1}\left(\begin{bmatrix} \dot{x}_P^* \\ \dot{y}_P^* \end{bmatrix} + \begin{bmatrix} \rho_x^* \\ \rho_y^* \end{bmatrix}\right), \tag{34}$$

with,

$$\dot{x}_P^* = |\upsilon_P + \Delta\upsilon_P|\cos(\theta_T^*), \quad \text{and} \quad \dot{y}_P = |\upsilon_P + \Delta\upsilon_P|\sin(\theta_T^*),$$

where $\Delta\upsilon_P = -k_\upsilon\|\mathbf{f}_\upsilon\| \leq \upsilon_P$, and $k_\upsilon(t)[m/(s.N)]$ is a physical constant that weighs the relation between the social force versus the velocity change. Additionally, the control errors are calculated through the following equations

$$\rho_x^* = l_x \tanh\left(\frac{k_x}{l_x}\tilde{x}^*\right), \quad \text{and} \quad \rho_y^* = l_y \tanh\left(\frac{k_y}{l_y}\tilde{y}^*\right),$$

where $\tilde{x}^* = x_P^* - x, \tilde{y}^* = y_P^* - y$, are the errors in the $\mathcal{X}$ and $\mathcal{Y}$ direction respectively, and consequently the desired orientation over the path is also modified and defined as θ_T^*. Note that the dynamic compensation, proposed in Sec. 3.1.2, must consider the modified kinematic references, i.e., $u_c \sim u_c^*$ and $\omega_c \sim \omega_c^*$. In this manner, the path-following over the free-collisions path is guaranteed.

5. Experimental Results

5.1. *Experimental setup*

With the purpose to obtain experimental results with human obstacles during the path-following, a structured scenario with a ceiling camera is considered. The algorithm consists in capturing a color image each sample time $t_s = 0.1\,\text{s}$ (according to computing speed $t_s \geq 0.03\,\text{s}$), where the posture of each individual, i.e., the human on the wheelchair and the human obstacle is characterized with the position of two color markers on their heads, which are different for each individual. For the purpose of this work, a sensory-system mounted in the robotic wheelchair, to detect and to track humans has been not considered necessary; however, future implementations could require extra sensory capacity, which has not been the focus of this study. Kinect cameras, Lidar and sensor fusion techniques could be useful to develop a final implementation of the prototype.

5.1.1. *Robotic Wheelchair prototype*

In this work, it is used a robotic wheelchair, which has been developed at the Technical University Ambato (see Fig. 7). The wheelchair has two independently driven wheels by two direct current motors (in the center part), and four caster wheel around the central axis conferring greater stability to the human–wheelchair

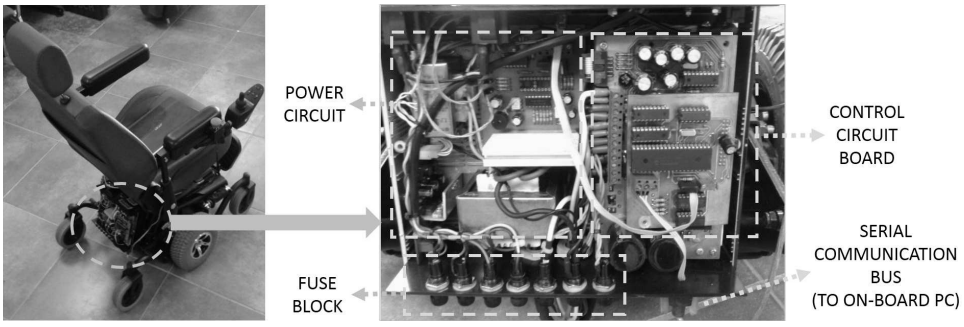

Fig. 7. Autonomous robotic wheelchair.

system (two in the rear part and two in the front part). Encoders installed on each one of the motor shafts allow knowing the relative position and orientation of the wheelchair.

Information provided by the encoders is used by the PID controllers responsible for getting an independent velocity control of the left and the right wheel. The hardware architecture of the robotic wheelchair consists of: (i) a commercial powered wheelchair from which only the mechanical structure and motors are used; the power card and joystick were discarded; (ii) two encoders directly connected to the motors; (iii) a microcontroller where the low-level velocity controller is implemented; (iv) a power card that amplifies PWM signals obtained from the microcontroller and sends them to the motors; (v) a computer where the high-level control algorithms and signal processing of the human–machine interface are implemented. The high-level controller is implemented under the Windows operating system using Microsoft Visual C++. The block diagram of the low-level velocity controller is shown in Fig. 8.

In this section, several experiments were executed to show the performance of the proposed controller and dynamic modeling of the human–machine system. These experiments are based on the wheelchair presented in Fig. 7.

The experimental platform uses a Labview HMI, which allows to capture and save experimental data and to send commands to the robotic wheelchair (see Fig. 9).

5.2. *Identification and validation of the proposed model*

Using this interface, the identification and validation procedures are done over the proposed model. For this, experimental data for identification and validation procedures is shown in Figs. 10 and 11 respectively, where it can be seen the good performance of the obtained dynamic model. The identification of the human–wheelchair system was performed by using least squares estimation applied to a filtered regression model.[34,35] The identified of dynamic parameters of the human–wheelchair system with a human of 73 [kg] are: $\chi_1 = 0.4903$, $\chi_2 = 0.2112$, $\chi_3 = -0.0011$, $\chi_4 = 1.0203$, $\chi_5 = 0.0346$, $\chi_6 = 0.9766$, $\chi_7 = -0.0016$ and $\chi_8 = -0.1001$.

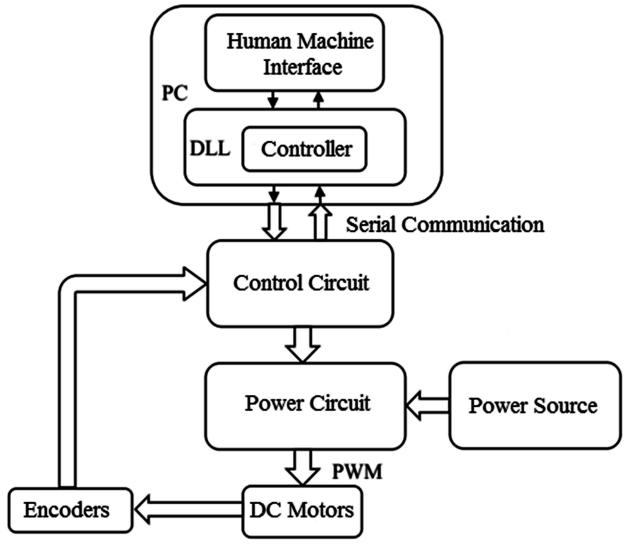

Fig. 8. Mechatronics architecture of the robotic wheelchair.

5.3. *Path-following control*

Three interference scenarios are considered, which validate the performance of the proposed algorithm. The parameters are adjusted as shown in Table 3. These values were selected by considering proxemic criteria and experimental values found in the

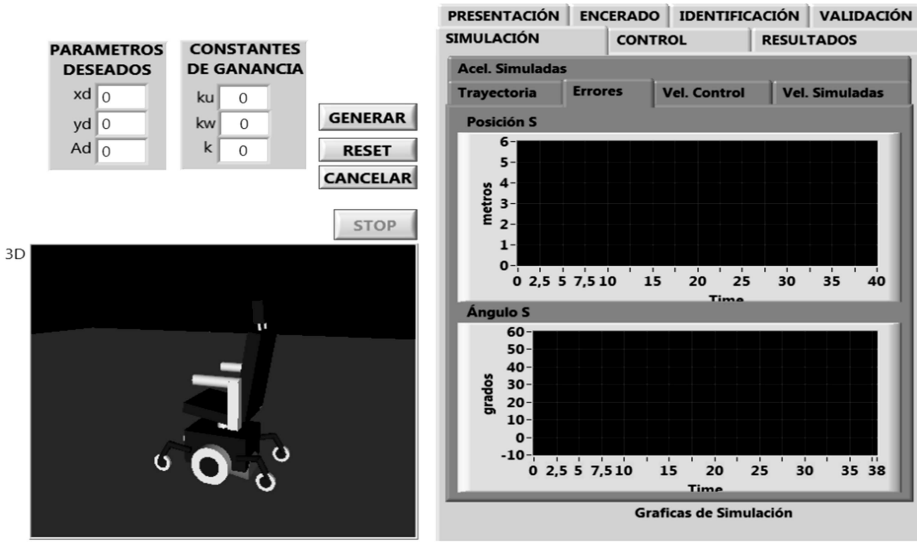

Fig. 9. Human–machine interface developed for the analysis of the model and the performance of the controller proposed.

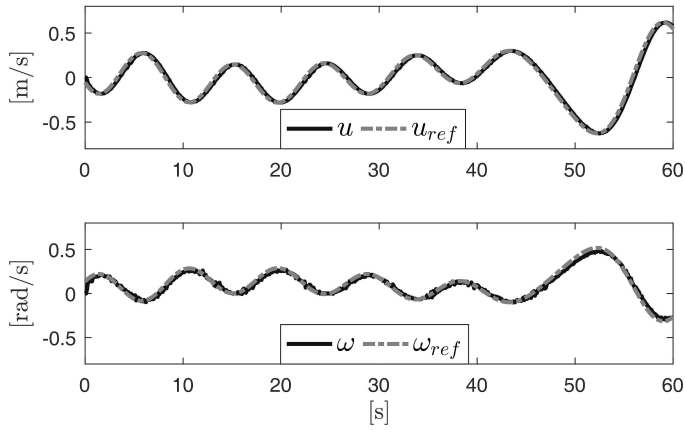

Fig. 10. Identification data for the proposed dynamic model. The solid lines represent the experimental velocities of the human–wheelchair system, and the dashed lines are the velocity references given to the robotic wheelchair.

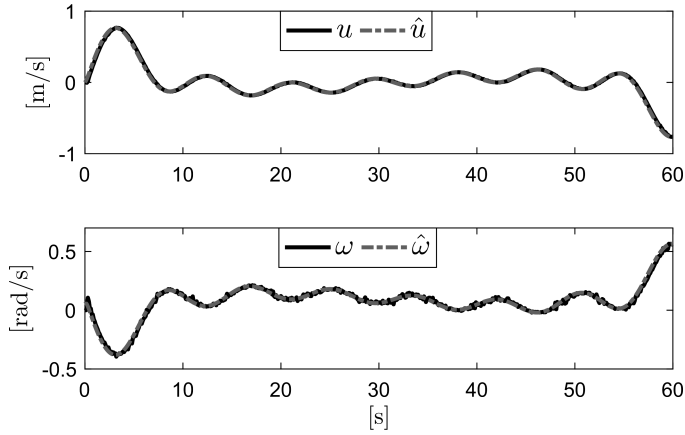

Fig. 11. Validation data of the proposed dynamic model. The dashed lines represent the proposed dynamic model signals and the solid lines are the experimental velocities of the human–wheelchair system.

Table 3. Parameters used during the experiments.

	Parameters	
Path-following control	$l_x = 0.5$	$k_x = 0.5$
	$l_y = 0.5$	$k_y = 0.5$
Ficticious force	$a = 1$	$b = 1$
Evasion effects	$k_N = 5$	$k_u = 0.1$
Social zone of the human obstacle	$m_a = 1$	$m_i = 0.6$
Security zone of the human–wheelchair system	$r = 0.3$	
Dynamic compensation	$l_\omega = 1$	$k_\omega = 0.25$
	$l_v = 2$	$k_v = 0.3$

bibliography.[36,37] However, all of them must be adjusted under the criteria of the designer, and by using trial-and-error process until getting the best performance of the algorithm. For these three cases, it is considered a linear path on the $\mathcal{X}$-axis, i.e., $y = 0$, and defined between $x \in [-1, 2]$. The human obstacles move without a previously marked path.

5.4. *Experiment* 1: *Interference in* 0°

This first experiment considers an interference case in 0°, commonly denominated *passing*, which is usual in corridors.

In this case, the expected behavior is given by a modulation of direction of the wheelchair during the evasion, and in some cases, it could result necessary to modulate slightly the longitudinal velocity.

In Fig. 12, it is shown the trajectory of the human–wheelchair system and the human obstacle. Note that, the wheelchair-system avoids the human with a strong change of direction during the evasion. At $t = 3\,\text{s}$, the robotic wheelchair starts the avoidance by turning left and reducing weakly the linear velocity, which is evident in $t = 6\,\text{s}$. Later, approximately at $t = 9\,\text{s}$, the convergence of the wheelchair into the path shows the good performance of the path-following control. Due to the fact that the path is defined in $y = 0, x \in [-1, 2]$, i.e., on the $\mathcal{X}$-axis, in consequence $\theta_T = 0$ at least during noncollision cases and the orientation error results to be $\tilde{\theta} = -\psi$. Therefore, the convergence errors to the path and orientation of the human–wheelchair system are shown in Fig. 13.

The collision avoidance behavior is efficiently quantified with the behavior factor τ, which is generated with the proposed inference system. The effects of the social evasion over the wheelchair/path are shown in Fig. 14.

Note that the behavior factor has values close to one during the evasion. This effect shows the system priorities to modulate the direction over the velocity.

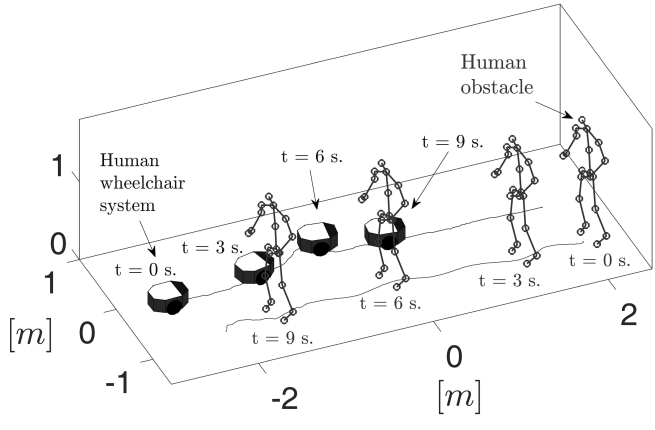

Fig. 12. Trajectory of the human–wheelchair system and the human obstacle.

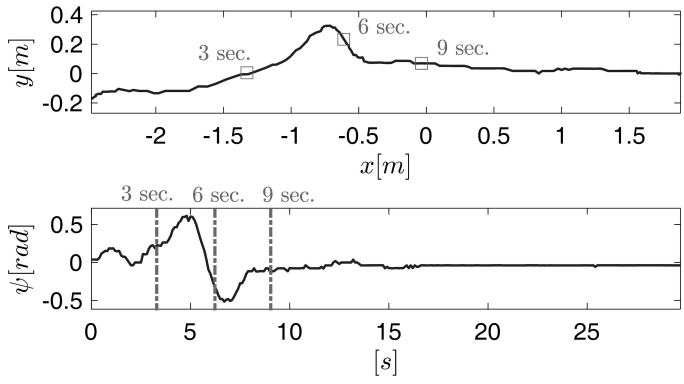

Fig. 13. Trajectory and orientation of the human–wheelchair system.

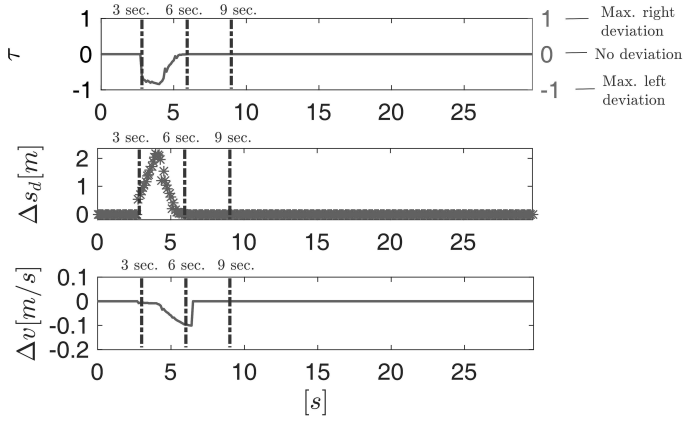

Fig. 14. Defuzzified behavior factor and effects over the system.

Finally, the measured linear and angular velocities of the wheelchair (dashed lines), and the control actions (solid lines) given to the system are shown in Fig. 15. There are some strong direction changes during the evasion and short periods of velocity changes, which attend to the desired behavior.

5.5. *Experiment* 2: *Interference in* 45°

In this second experiment, a 45° interference is considered, which is usual in intersections of paths. In this case, the expected behavior considers to prioritize velocity modulation during the evasion, and if possible, the human wheelchair system *moves behind* the human obstacle, i.e., robot waits and passes behind him/her.

In Fig. 16, the trajectory of the human–wheelchair system and the human obstacle during the evasion are presented, where the good performance of the

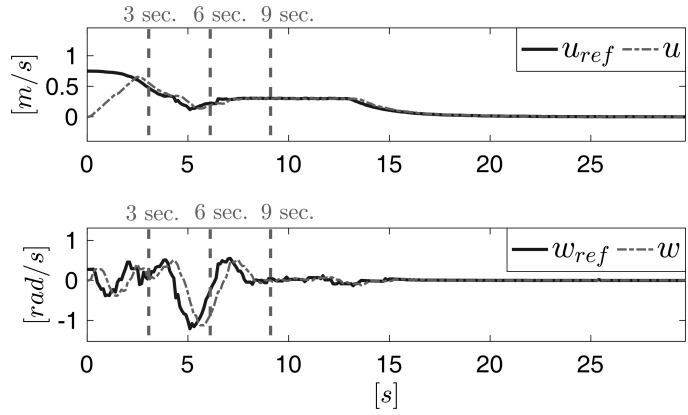

Fig. 15. Robotic wheelchair velocities (dashed lines) and control actions (solid lines).

path-following control is also verified. Due to the path is defined in $y = 0, x \in [-1, 2]$, i.e., on the $\mathcal{X}$-axis, in consequence $\theta_T = 0$ at least during noncollision cases and the orientation error results to be $\tilde{\theta} = -\psi$. Note that, the wheelchair-system avoids the human with a strong change of velocity during the evasion. At $t = 4\,\text{s}$, the robotic wheelchair is reducing its velocity and a weakly change of direction to move behind the human is produced at approximately $t = 6\,\text{s}$, the convergence of the wheelchair into the path shows the good performance of the path-following control. Therefore, the convergence errors to the path and the orientation of the wheelchair system are shown in Fig. 17.

This behavior is quantified through the defuzzified behavior factor τ and the social evasion effects over the robot/path system are shown in Fig. 18.

Note that the behavior factor has values close to zero during the evasion. This effect shows that the system prioritizes to modulate velocity over direction.

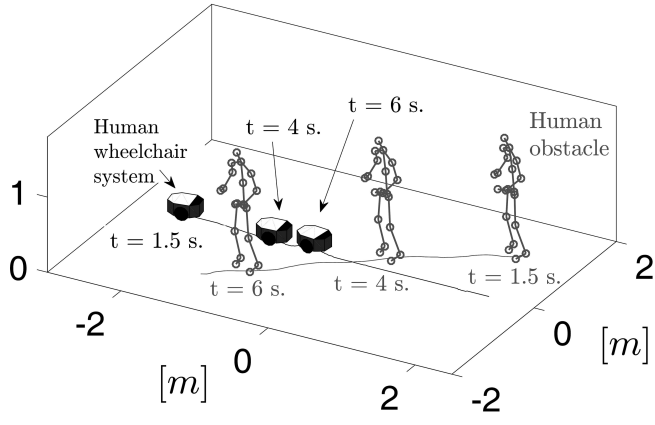

Fig. 16. Trajectory of the human–wheelchair system and the human obstacle.

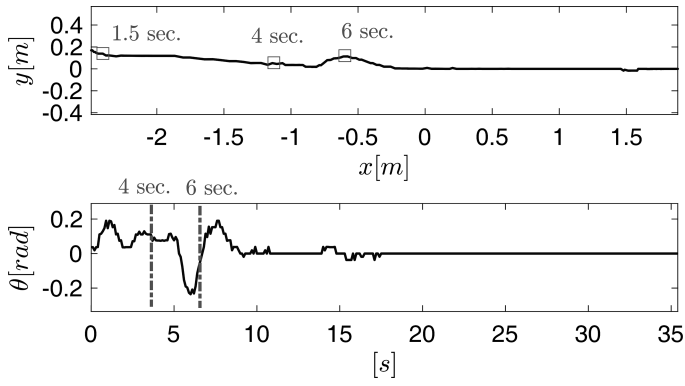

Fig. 17. Trajectory and orientation of the human–wheelchair system.

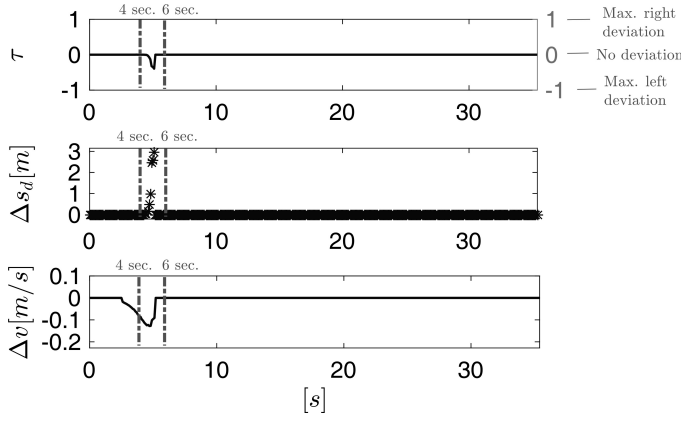

Fig. 18. Defuzzified behavior factor and effects over the system.

Finally, the measured linear and angular velocities of the wheelchair (dashed lines), and the control actions (solid lines) given to the system are shown in Fig. 19 where it is shown a strong velocity modulation during the evasion.

5.6. *Experiment* 3: *Interference in* 90°

Finally, in this last experiment, a 90° interference is considered. This is commonly denominated *crossing situation*, which is usually found in intersections of paths.

In this case, the desired behavior considers a velocity modulation and a direction change during the evasion. A *move behind* the human obstacle could be necessary when the conditions request it.

In Fig. 20, the trajectory of the robotic wheelchair and the human obstacle during the evasion are presented. Note that, during this situation, the human–wheelchair

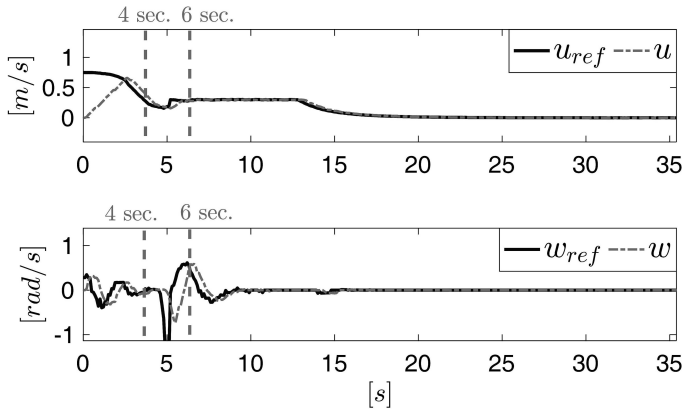

Fig. 19. Robot velocities (dashed lines) and control actions (solid lines).

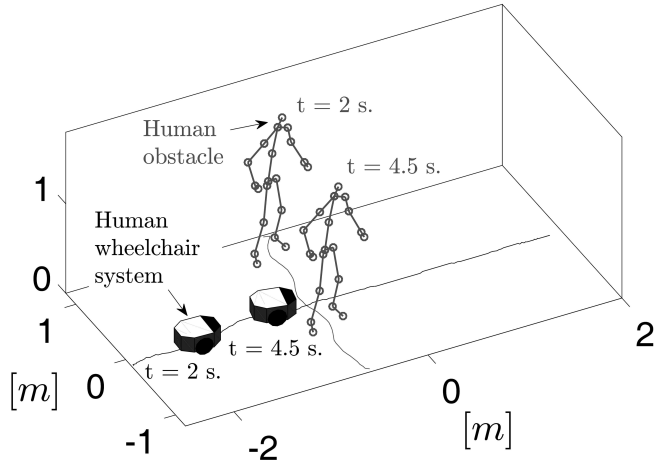

Fig. 20. Trajectory of the human–wheelchair system and the human obstacle.

system turns left slightly to avoid the human, but the collision is mainly avoided with a longitudinal velocity modulation. At $t = 2\,\mathrm{s}$, the robotic wheelchair is turning left and starts a longitudinal velocity reduction. At $t = 4.5\,\mathrm{s}$, the wheelchairs moves to the path and the good performance of the path-following control is verified. Due to the path is defined in $y = 0, x \in [-1, 2]$, i.e., on the $\mathcal{X}$-axis, $\theta_T = 0$ at least during noncollision cases and the orientation error results to be $\tilde{\theta} = -\psi$. Therefore, the convergence errors to the path can be shown in Fig. 21.

This behavior is efficiently quantified through the behavior factor τ, which is generated by the fuzzy-inference system and the effects over the system wheelchair/path are shown in Fig. 22.

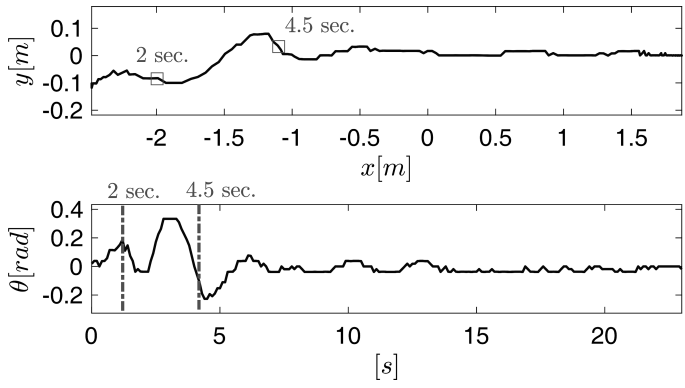

Fig. 21. Trajectory and orientation of the human–wheelchair system.

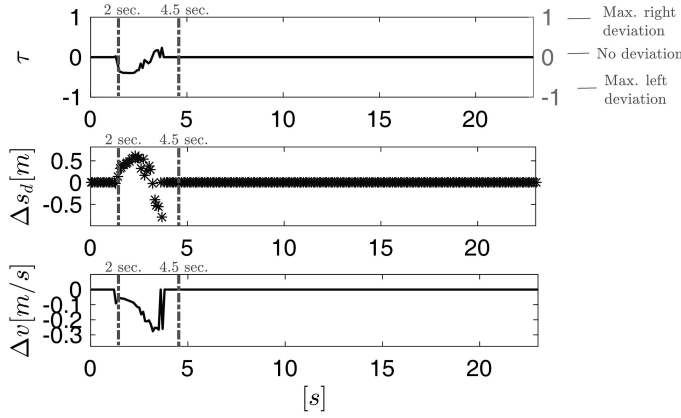

Fig. 22. Defuzzified behavior factor and effects over the system.

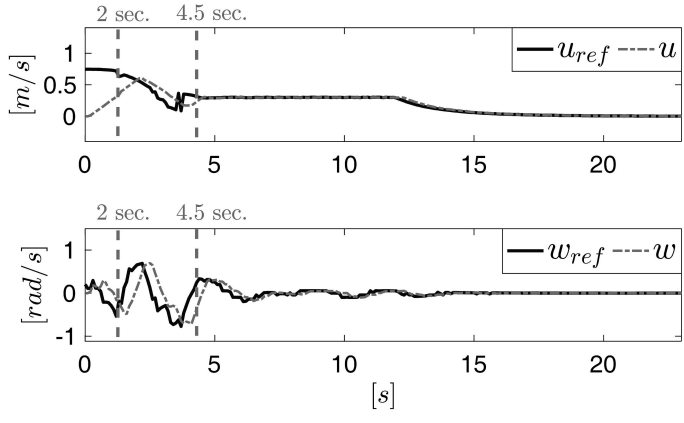

Fig. 23. Robot velocities (dashed lines) and control actions (solid lines).

Note that the behavior factor has values between 0 and 1 during the evasion, i.e., there is not a predominant effect in this case. In this way, the system modulates velocity but also direction during the evasion by generating a motion of *moving behind* the human obstacle.

Finally, the control actions given to the robotic wheelchair and its measured velocities are shown in Fig. 23, where a balance between a slight velocity modulation and a slight deviation is shown during the evasion of the human obstacle.

6. Discussion

The good performance of the approach has been verified through three experiments with three different interference cases. At first, the good performance of the path-following control algorithm with the experimental platform has shown that the robot is capable of following the path while compensating all the dynamic effects because of the human position changes into the wheelchair. Later, the results obtained with the fuzzy logic methodology for human evasion demonstrate that the system has been able to make difference between the different interference situations; and the selection of its corresponding collision avoidance strategy has been chosen as expected. During all the cases, a successfully human-collision avoidance and a good performance of the path following control was tested. Note that, the good performance of the path-following control is crucial to guarantee the good performance of the pedestrian collision evasion.

7. Conclusions

In this paper, the modeling and control of the human–wheelchair system by considering lateral deviations of the center of mass was proposed. This approach considers velocity commands as control signals of the system. The proposed controller resolves the path following problem control for a robotic wheelchair, which is also capable of positioning the human–wheelchair system. The design of controller is based on two cascaded subsystems: a kinematic controller which complies with the task objective (path following and positioning), and a dynamic controller that compensates the dynamics of the human–wheelchair system. Additionally, a fuzzy-based quantification of social rules in pedestrian collision avoidance scenarios is included. It allows the identification of different behaviors, i.e., adjustments of wheelchair velocity or path when avoiding collisions with humans. For this reason, a social force composition and its incorporation in the aforementioned path-following scenario is presented. Finally, the stability of the control system is proved by considering the Lyapunov's method, and the performance of the proposed controller is shown through real experiments. Future works will be focused on considering the compensation of other dynamic problems in the navigation of the human–wheelchair system, like slipping in sloping and greasy surfaces as well as unexpected rugged

terrain. Additionally, further modifications will be oriented to overcome crowds dynamics, which usually result a key challenge during human–robot interaction regarding to the scalability during pedestrians collision avoidance.

Acknowledgments

The authors would like to thank Technical University of Ambato, University of the Arms Forces (ESPE) and the Institute of Automatics of the National University of San Juan, for the support to develop this work.

References

1. T. F. Bastos-Filho, F. A. Cheein, S. M. T. Müller, W. C. Celeste, C. de la Cruz, D. C. Cavalieri, M. Sarcinelli-Filho, P. F. S. Amaral, E. Perez, C. M. Soria and R. Carelli, Towards a new modality-independent interface for a robotic wheelchair, *IEEE Trans. Neural Syst. Rehabil. Engrg.* **22**(3) (2014) 567–584.
2. Y. Wang and W. Chen, Hybrid map-based navigation for intelligent wheelchair, in *IEEE Int. Conf. Robotics and Automation*, May 2011, pp. 637–642.
3. W. C. Cheng and C. C. Chiang, The development of the automatic lane following navigation system for the intelligent robotic wheelchair, in *IEEE Int. Conf. Fuzzy Systems* (*FUZZ-IEEE 2011*), June 2011, pp. 1946–1952.
4. K. Biswas, O. Mazumder and A. S. Kundu, Multichannel fused emg based biofeedback system with virtual reality for gait rehabilitation, *4th Int. Conf. Intelligent Human Computer Interaction* (*IHCI*), December 2012, pp. 1–6.
5. Y. Munakata, A. Tanaka and M. Wada, A five-wheel wheelchair with an active-caster drive system, in *IEEE 13th Int. Conf. Rehabilitation Robotics* (*ICORR*), June 2013, pp. 1–6.
6. J. Yuan, Stability analyses of wheelchair robot based on human-in-the-loop control theory, in *2008 IEEE Int. Conf. Robotics and Biomimetics*, Feb 2009, pp. 419–424.
7. M. Mazo, J. García, F. Rodríguez, J. U. na, J. Lázaro and F. Espinosa, Integral system for assisted mobility, *Inf. Sci.* **129** (2000) 1–15.
8. Q. Zeng, C. L. Teo, B. Rebsamen and E. Burdet, A collaborative wheelchair system, *IEEE Trans. Neural Syst. Rehabil. Eng.* **16**(2) (2008) 161–170.
9. S. P. Parikh, V. G. Jr., V. Kumar and J. O. Jr., Integrating human inputs with autonomous behaviors on an intelligent wheelchair platform, *IEEE Intell. Syst.* **22**(2) (2007) 33–41.
10. C. D. L. Cruz, T. F. Bastos and R. Carelli, Adaptive motion control law of a robotic wheelchair, *Control Eng. Practice* **19**(2) (2011) 113–125.
11. D. Soetanto, L. Lapierre and A. Pascoal, Adaptive, non-singular path-following control of dynamic wheeled robots, *42nd IEEE Int. Conf. Decision and Control*, Vol. 2, December 2003.
12. X. Yuhua, Z. Chongwei, B. Wei and T. Lin, Dynamic sliding mode controller based on particle swarm optimization for mobile robot's path following, in *2009 Int. Forum on Information Technology and Applications*, Vol. 1, May 2009, pp. 257–260.
13. S. Wangmanaopituk, H. Voos and W. Kongprawechnon, Collaborative nonlinear model-predictive collision avoidance and path following of mobile robots, in *2009 ICCAS-SICE*, August 2009, pp. 3205–3210.

14. Y. Tanimoto, K. Namba, K. Furusawa, H. Yamamoto, A. Tokuhiro and H. Ukida, Imaging of the turn space and path of movement of a wheelchair for remodeling houses of individuals with sci, *IEEE Int. Conf. Imaging Systems and Techniques Proceedings*, July 2012, pp. 309–314.
15. S.-H. Chen and J.-J. Chou, Motion control of the electric wheelchair powered by rim motors based on event-based cross-coupling control strategy, in *2011 IEEE/SICE Int. Symp. System Integration* (*SII*), December 2011, pp. 1340–1345.
16. F. N. Martins, W. C. Celeste, R. Carelli, M. Sarcinelli-Filho and T. F., Bastos-Filho, An adaptive dynamic controller for autonomous mobile robot trajectory tracking, *Control Eng. Practice* **16**(11) (2008) 1354–1363.
17. S. Z. Yahaya, R. Boudville, M. N. Taib and Z. Hussain, Dynamic modeling and control of wheel-chaired elliptical stepping exercise, *2012 IEEE Int. Conf. Control System, Computing and Engineering*, November 2012, pp. 204–209.
18. B. Sapey, J. Stewart and G. Donaldson, Increases in wheelchair use and perceptions of disablement, in *Disability and Society*, 2005, pp. 489–505.
19. C.-P. Lam, C.-T. Chou, K.-H. Chiang and L.-C. Fu, Human centered robot navigation towards a harmoniously human robot coexisting environment, *IEEE Trans. Robotics* **27**(1) (2011) 99–112.
20. L. Scandolo and T. Fraichard, An anthropomorphic navigation scheme for dynamic scenarios, in *IEEE Int. Conf. Robotics and Automation* (*ICRA*), 2011, pp. 809–814.
21. J. Guzzi, A. Giusti, L. M. Gambardella, G. Theraulaz and G. A. Di Caro, Human-friendly robot navigation in dynamic environments, in *IEEE Int. Conf. Robotics and Automation* (*ICRA*), 2013, pp. 423–430.
22. P. Ratsamee, Y. Mae, K. Ohara, T. Takubo and T. Arai, Human-robot collision avoidance using a modified social force model with body pose and face orientation, *Int. J. Huma. Robot.* **10**(1) (2013) 1350008.
23. D. Helbing and P. Molnár, Social force model for pedestrian dynamics, *Phys. Rev. E* **51**(5) (1995) 4282–4286.
24. M. Moussaïd and J. D. Nelson, Simple heuristics and the modelling of crowd behaviours, *Pedestrian and Evacuation Dynamics 2012* (Springer International Publishing, Switzerland, 2014), pp. 75–90.
25. T. Kruse, P. Basili, S. Glasauer and A. Kirsch, Legible robot navigation in the proximity of moving humans, *IEEE Workshop on Advanced Robotics and its Social Impacts*, 2012, pp. 83–88.
26. T. Kruse, A. Kirsch, H. Khambhaita and R. Alami, Evaluating directional cost models in navigation, *ACM/IEEE Int. Conf. Human-Robot Interaction*, 2014, pp. 350–357.
27. J. Guzzi, A. Giusti, L. M. Gambardella and G. A. Di Caro, Local reactive robot navigation: A comparison between reciprocal velocity obstacle variants and human-like behavior, *IEEE/RSJ Int. Conf. Intelligent Robots and Systems* (*IROS*), 2013, pp. 2622–2629.
28. M. Moussaïd, D. Helbing and G. Theraulaz, How simple rules determine pedestrian behavior and crowd disasters, *Proc. Natell. Acad. Sci.* (2011).
29. K.-E. Ko and K.-B. Sim, Imitative neural mechanism-based behavior intention recognition system in humanrobot interaction, *Int. J. Humanoid Robot.* **11**(04) (2014) 1442008.
30. Y. Zhang, D. Hong, J. H. Chung and S. A. Velinsky, Dynamic model based robust tracking control of a differentially steered wheeled mobile robot, in *Proc. 1998 American Control Conf.*, Vol. 2, June 1998, pp. 850–855.

31. V. H. Andaluz, P. Canseco, J. Varela, J. S. Ortiz, M. G. Pérez, V. Morales, F. Roberti and R. Carelli, *Modeling and Control of a Wheelchair Considering Center of Mass Lateral Displacements* (Springer International Publishing, Switzerland, 2015).
32. M. Huber, Y.-H. Su, M. Krüger, K. Faschian and S. Glasauer, Adjustments of speed and path when avoiding collisions with another pedestrian, *PLoS ONE* **9**(02) (2014) e89589.
33. G. Arechavaleta, J.-P. Laumond, H. Hicheur and A. Berthoz, The nonholonomic nature of human locomotion: A modeling study, in *IEEE/RAS-EMBS Int. Conf. Biomedical Robotics and Biomechatronics*, February 2006, pp. 158–163.
34. K. J. Astrom and B. Wittenmark, *Adaptive Control*, 2nd edn. (Addison-Wesley Longman Publishing Co., Inc., Boston, 1994).
35. F. Reyes and R. Kelly, On parameter identification of robot manipulators, in *Proc. Int. Conf. Robotics and Automation*, Vol. 3, April 1997, pp. 1910–1915.
36. E. Pacchierotti, H. I. Christensen and P. Jensfelt, Evaluation of passing distance for social robots, *15th IEEE Int. Symp. Robot and Human Interactive Communication*, 2006, pp. 315–320.
37. E. T. Hall, A system for the notation of proxemic behavior, *Am. Anthropol.* **65**(5) (1963) 1003–1026.

Daniel Herrera was born in Riobamba, Ecuador, in 1989. He received his degree in Electronic and Control Engineering from the National Polytechnic School of Ecuador in 2012, where he was also Laboratory Assistant at the Department of Automation and Industrial Control. He obtained a Ph.D. degree in Control Systems Engineering at the Institute of Automatics (INAUT) of the National University of San Juan, Argentina in March 2017.

Currently, he is a Postdoctoral Researcher at INAUT. His research interests are human–robot interactions, artificial intelligence and robots modeling.

Flavio Roberti was born in Buenos Aires, Argentina in 1978. He graduated in Engineering from the National University of San Juan, Argentina in 2004, and obtained a Ph.D. degree in Control Systems Engineering from the National University of San Juan, Argentina in 2009. He is currently an Assistant Professor at the National University of San Juan and a Researcher of the National Council for Scientific and Technical Research (CONICET, Argentina). His research interests are robotics, wheeled mobile robots, mobile manipulators, visual servoing and passivity-based visual control.

Ricardo Carelli was born in San Juan, Argentina. He graduated in Engineering from the National University of San Juan, Argentina, and obtained a Ph.D. degree in Electrical Engineering from the National University of Mexico (UNAM). He is a Full Professor at the National University of San Juan and a Senior Researcher of the National Council for Scientific and Technical Research (CONICET, Argentina). Professor Carelli is the Director of the Instituto de Automática, National University of San Juan (Argentina).

His research interests are in robotics, manufacturing systems, adaptive control and artificial intelligence applied to automatic control. Professor Carelli is a Senior Member of IEEE and a Member of AADECA-IFAC.

Victor Andaluz was born in Ambato-Ecuador in 1984. He obtained a Ph.D. in Control Systems Engineering in 2011. Currently, he is working at the Universidad de las Fuerzas Armadas ESPE, Latacunga-Ecuador. His area of research is intelligent control applied to production systems, mobile robots and rehabilitation of people disabilities.

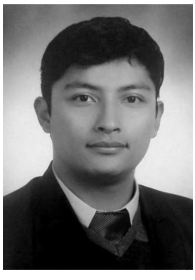

José Varela was born in Ambato-Ecuador in 1990. He obtained a Master's degree in Industrial Control and Automation Systems in 2016. Currently, he is working at the Universidad de las Fuerzas Armadas ESPE. He is working in robotics, modeling and identification of nonlinear systems, intelligent control, simulation of systems in multiple environments and SCADA's.

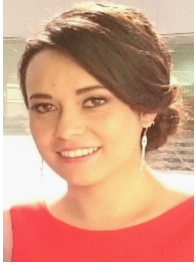

Jessica Ortiz graduated in Electronic Engineering in Control and Industrial Networks at the Escuela Superior Politécnica de Chimborazo in 2013, also obtained a Master's degree in Industrial Control and Automation Systems in 2016. Areas of interest are control systems, industrial automation and virtual reality.

Paúl Canseco graduated in Electronic Engineering in Control at the Escuela Politécnica Nacional (EPN) in 2011. Currently, he is studying a Master degree in Electronic Design at the Beijing University of Technology, China. His areas of interest are power systems, industrial automation and control system.